EXPLORING THE POTENTIAL ENERGY SURFACE OF Au_{55} MAGIC CLUSTER TO STUDY THERMODYNAMIC PROPERTIES

M.Sc. Thesis

By

VIKAS SONI

(1603131020)

DISCIPLINE OF CHEMISTRY

INDIAN INSTITUTE OF TECHNOLOGY INDORE

JUNE, 2018

EXPLORING THE POTENTIAL ENERGY SURFACE OF Au_{55} MAGIC CLUSTER TO STUDY THERMODYNAMIC PROPERTIES

A THESIS

Submitted in partial fulfillment of the
requirements for the award of the degree
of
Master of Science

by

VIKAS SONI

DISCIPLINE OF CHEMISTRY
INDIAN INSTITUTE OF TECHNOLOGY INDORE
JUNE, 2018

INDIAN INSTITUTE OF TECHNOLOGY INDORE

CANDIDATE'S DECLARATION

I hereby certify that the work which is being presented in the thesis entitled **EXPLORING THE POTENTIAL ENERGY SURFACE OF Au_{55} MAGIC CLUSTER TO STUDY THERMODYNAMIC PROPERTIES** in the partial fulfillment of the requirements for the award of the degree of **MASTER OF SCIENCE** and submitted in the **DISCIPLINE OF CHEMISTRY, Indian Institute of Technology Indore**, is an authentic record of my own work carried out during the time period from July 2017 to July 2018 under the supervision of Dr. Satya S. Bulusu, Assistant Professor, Indian Institute of Technology Indore, India.

The matter presented in this thesis has not been submitted by me for the award of any other degree of this or any other institute.

(VIKAS SONI)

This is to certify that the above statement made by the candidate is correct to the best of my knowledge.

(Dr. Satya S. Bulusu)

VIKAS SONI has successfully given his/her M.Sc. Oral Examination held on _____.

Signature of Supervisor of MSc thesis
Date:

Convener, DPGC
Date:

Signature of PSPC
Date:

Signature of PSPC
Date:

ACKNOWLEDGEMENTS

I would like to thank my supervisor, ***Dr. Satya S. Bulusu***, for the patience guidance, encouragement and advice he has provided throughout my time as his student. I have been extremely lucky to have a supervisor who cared so much about my work, and who responded to my questions and queries so promptly. I would like to thank my PSPC members ***Dr. Anjan Chakraborty*** and ***Dr. Srivathsan Vasudevan***.

I want to acknowledge the assistance of my lab seniors Shweta Jindal, S. Chiriki and Priya Singh in helping work out some of the specific problems and in providing their constant support during the whole project. I cannot forget the valuable help and motivation of my senior Shweta Jindal specially.

I also thank my roommates Vishal Budhija and Agnideep Das for favoring me in all situations. I am also grateful to Arun Tiger, Dondi Deori (H.G.), P. Yadav and Baman KS Pandey and all classmates (especially all boys), batch mates and seniors in other labs, for their continuous support and encouragement. I also thank my M.Sc. seniors Manjeet (Sardar), Amit (Jugnoo) and A. Bharti (SK).

Finally, I address the people who mean a lot to me, my parents, MAA and BAPU, for showing faith in me and giving me freedom to choose what I desired. I salute you all for the selfless love, care, pain and sacrifice you did to shape my life. Although you hardly understood what I researched on, you were willing to support any decision I made. I would never be able to pay back the love and affection showered upon by my parents.

Thanks to my both sisters Preeti and Poonam for their selfless love, care and dedicated efforts which contributed a lot for completion of my thesis.

I would like to offer special thanks to my Mama ji Sh. Vijender Singh, who, although no longer with us, continues to inspire me by his past experiences.

Last but not the least, I would like to acknowledge my brothers Saurabh Sharma (Guru Ji) and Amit Soni (Baba Ji) for supporting me in the worst phases of life.

VIKAS SONI

DISCIPLINE OF CHEMISTRY

IIT INDORE

IN THE MEMORY OF MY BELOVED MAMA JI

Abstract

For the large size nanoclusters (equivalent diameter of 1.0 nm to 4.0 nm), finding the global minimum (GM) is a major challenge in chemistry, physics and biosciences due to high computational cost required to explore their potential energy surface (PES). The structure, reactivity, properties and spectra of the chemical system can be easily studied with the help of PES. Herein, we have done the PES fitting using two body function i.e. spherical harmonics based descriptor integrated with artificial neural network (ANN). We have performed the molecular dynamics (MD) simulations and GM optimization for Au_{55} by using ANN and found that the GM is an amorphous molecular structure rather than icosahedron geometry (ICO). Using DFT, we have confirmed that the predicted GM is 2.22 eV lower in energy than ICO. The predicted GM consists of 8 atoms in the core and 47 atoms on the surface. A brief study on fluxional nature and probability of low-lying isomers of Au_{55} is performed and it is concluded that Au_{55} has a dynamic surface which can be helpful in the study of reaction dynamics. Also, GM structure is stable up to a high temperature of 750 K.

TABLE OF CONTENTS

LIST OF FIGURES

LIST OF TABLES

NOMENCLATURE

α	Alpha
β	Beta
η	Eta
θ	Angle
κ	Kappa
π	Pi
Å	Angstrom
K	Kelvin
σ	Sigma
eV	electron volt
I	Moment of Inertia
%	Percentage
γ	Gamma

ACRONYMS

PES	Potential Energy Surface
Au	Gold
MD	Molecular Dynamics
GM	Global Minimum
ANN	Artificial Neural Network
NCs	Nanoclusters
DNA	Deoxyribonucleic acid
ICO	Icosahedral
HL	Hidden layer
BFGS	Broyden-Fletcher-Goldfarb-Shanno
VASP	Vienna Ab initio Simulation package
PBE	Perdew-Burke-Ernzerhof
GGA	Generalised Gradient Approximation
BH	Basin Hoping
SOC	Spin Orbit Coupling
vdW	Van der Waals

Chapter 1

Introduction

1.1. General Introduction:

Gold is, indeed, a unique element and shows characteristically different structural and electronic properties due to very large relativistic effects *[1, 2]* among other elements with atomic number less than 100. Some of the observed outcomes *[3]* of relativistic effects are (a) Reduction in the gap between 6s and 5d orbitals, (b) Expansion of 5d orbitals and contraction of 6s orbitals, and (c) A significant s-d hybridization. Also, gold nanoclusters (NCs) have different promising applications in bio labeling *[4]*, catalysis *[5]*, nanoscale devices *[6]*, molecular imaging *[7]*, DNA melting *[8]*. So, to investigate the dynamical, structural, electronic, and other physical and chemical properties of gold NCs, the knowledge of NCs geometry is the preliminary requirement. Exploration of PES gives the information of the geometries which are trapped in a local minima, as well as the geometry of the global minimum *[9]*. For a periodic system, the GM provides the crystalline ground state configuration of a solid. With the help of the GM geometry, various physical and chemical properties like charge state, type of interactions between atoms, surface energy contribution, catalytic behavior, size, shape, kinetics effect, energetic effects, optical properties, magnetic properties, can be easily explained.

As experimental determination of the geometric ground state of complex system is very difficult, theoretical study using simulation methods is a promising candidate for the determination of the structure of such complex systems *[9]*. For example, a number of unknown alloy *[10, 11]* structures were recently identified by simulation methods. For the large size NCs, the GM search becomes computationally expensive because the number of local minima increases exponentially with respect to the number of atoms in the system. In order to reach the GM, the system has to overcome the

barriers separating the local minima. The crossover of the barriers is achieved mostly by using the algorithms which are based on the thermodynamic principles *[12-14]*.

In this work, we have done the fitting of PES for a range of Au clusters (Au_{13}- Au_{60}) using the technique of ANN potential *[15]*. We have used the spherical harmonics descriptors *[16]* as inputs to the ANN. We have explored the PES for Au_{55} system and have found its probable GM structure. Au_{55} is a magic cluster, and initially, it was assumed to be relatively stable due to the formation of the closed shell Mackay 55-atom icosahedron structure with I_h symmetry *[17]*. Recent studies *[18- 20]* have showed that the ICO geometry does not make the GM structure. The obtained GM structure for Au_{55} system is not a symmetric structure like ICO structure. It adopts an amorphous geometry with a symmetric core and unsymmetrical surface. We have analyzed the dynamics of Au_{55} and have found that although being a magic cluster, Au_{55} does not exhibit an ICO geometry. We compared the geometry of the probable GM structure with the earlier reported GM by Piotrowski et al. *[18]* and found it to be completely different in the atomic arrangements. We have found that according to DFT calculations, the predicted GM is 2.22 eV lower in energy than the icosahedron geometry. The predicted GM is composed of 14.5% of core atom, while 85.5% of the atoms are located on the surface region. We have also studied the fluxional property and probability distribution for Au_{55}. The computational details can be found in section 2, followed by results and discussion in section 3 and conclusion in section 4.

1.2. Organization of thesis:

The aim of this project was to study PES of Au_{55} nanocluster and to find the GM structure. For this purpose, we ran extensive MD simulations integrated with ANN to understand thermodynamic properties of Au_{55}.

Chapter 2: This chapter describes the theory behind the work and the computational details.

Chapter 3: In this chapter, the detailed discussion of the results, is summarized.

Chapter 4: This chapter is the conclusion of the whole work and also describes the future scope and applications.

Chapter 2

Theory and Computational Details

2.1. Structure of ANN:

To construct a direct functional relation between the atomic configuration and the potential energy, we used ANN *[21]* with two hidden layers (HL) (Fig. 1). In the network, we are giving descriptors as input and getting the energy as the corresponding output. In the present study, to compute the energy of a cluster (Eq. 2), we have taken ANN comprising of input layer, HL one, HL two and output layer, and termed the network as a small feed forward neural network (NN) *[22]*. Each HL consists of 30 nodes. For a single atom, the network comprises of 2760 weights (N_w) and 59 input functions.

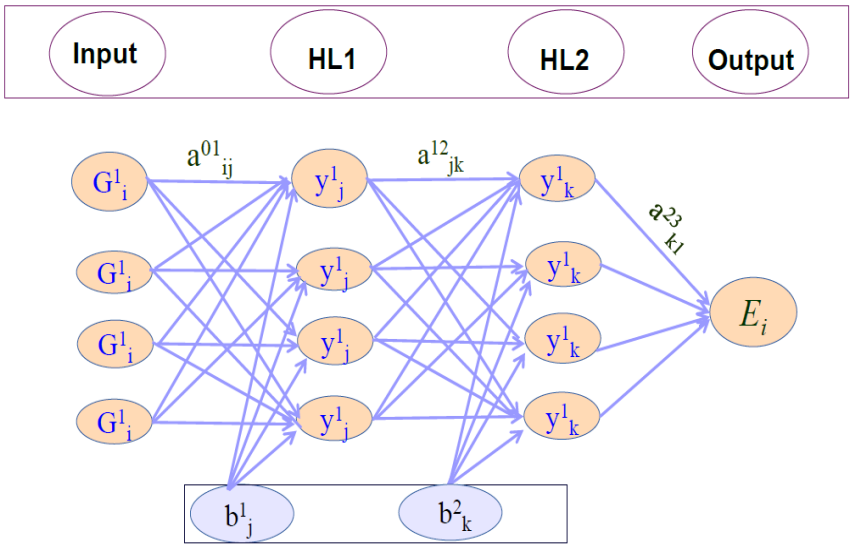

Figure 1: Schematic structure of a small feed-forward NN. The nodes are arranged in layers.

In the Fig.1, y^1 and y^2 represent the nodes of HL one and HL two, respectively. i, j and k are the number of nodes in input layer, HL one and HL two, respectively. The energy of x atom of a nanocluster is computed by ANN using the Eq.1,

$$E_x = \sum_{k=1}^{30} a_{kl}^{23} \cdot f_k^2 \left(b_k^2 + \sum_{j=1}^{30} a_{jk}^{12} \cdot f_j^1 \left(b_j^1 + \sum_{i=1}^{59} a_{ij}^{01} . G_{xi} \right) \right) \quad \ldots\ldots\ldots (1)$$

Here, a_{ij}^{01} , a_{jk}^{12} , a_{kl}^{23} represents the weights connecting from the input layer to hidden layer one, hidden layer one to hidden layer two, and hidden layer two to output layer, respectively. G_{xi} is the input descriptor functions which are 59 for an atom x. f_a and f_b represents the sigmoid function for activation of the network. b_j and b_k corresponds to the bias layer weights of the first and the second hidden layer, respectively. The total energy (E) of a nanoparticle is given by summing all the atomic energies,

$$E = \sum_{x}^{atoms} E_x \qquad \ldots\ldots\ldots (2)$$

To describe the local atomic environment for a cluster, we have to fit 3N forces along with one energy component. The analytical force can be given by negative gradient of total energy of the system w.r.t. Cartesian coordinates i.e.

$$F_{k,\alpha} = \frac{-\delta E}{\delta R_{k,\alpha}} \qquad \ldots\ldots\ldots (3)$$

2.2. Description of atomic environment:

To describe the local atomic environment of the structure, we have taken two type of functions – radial *[22]* and power spectrum coefficients *[21, 16]*. The radial function is a two body function which is given by the Eq.4,

$$G_i^{Rad} = \sum_{i \neq j} e^{-nR_{ij}^2} f_C(R_{ij}) \qquad \ldots\ldots\ldots (4)$$

Where, $f_c(R_{ij})$ is the cut-off function and is defined as,

$$f_c(R_{ij}) = 0.5\left\{\cos\left(\frac{\pi R_{ij}}{R_c}\right) + 1\right\} \qquad \ldots\ldots\ldots (5)$$

This cut-off function tends to zero when $R_{ij} \geq R_c$ and it has a finite value when $R_{ij} \leq R_c$. Here, R_{ij} stands for interatomic distance between i^{th} and j^{th}

atom and R_c for the cut-off radius. The power spectrum coefficients are spherical harmonics based descriptors and are given by,

$$G_i^{Ang} = \frac{4\pi}{2l+1} \sum_{m=-l}^{l} C_{nlm}^* C_{nlm} \quad \ldots\ldots\ldots (6)$$

Whereas, coefficients c_{nlm} are given by the Eq.7,

$$C_{nlm} = \sum_{i \neq j} e^{-\kappa R_{ij}^2} f_C(R_{ij}) Y_{lm}(r_{ij}) \quad \ldots\ldots\ldots (7)$$

Where, η stands for the Gaussian width and l for the angular quantum number. The values of η and κ are given in the Table 1 and Table 2 respectively. Y_{lm} represents the spherical harmonic function and its detail can be found in work done by Jindal et al. *[16]*. In the present work, we have taken 9 radial functions (G_i^{Rad}) and 50 power spectrum coefficients (with l = 10). So, for an atom, we have 59 input coefficients to ANN.

Table 1: The values of the parameter η.

η(Å^{-2})	0.005	0.015	0.023	0.038	0.060	0.090	0.150	0.260	0.480

Table 2: The values of the parameter κ.

κ(Å^{-2})	0.0028	0.0040	0.0110	0.0280	0.0590

2.3. Scaling of input values:

The inputs (G_{xi}) obtained using spherical harmonics descriptors, are of high values. Further, when we multiply G_{xi} with weights and takes its sigmoid (Eq.1), then again, it gives values of higher magnitude. These high values will lead to the deactivation of the ANN. So, to avoid saturation of the network, scaling of the descriptor is accomplished and input values are scaled in the range of 0 to 1 *[22]*.

2.4. Preparation of training data:

Monte Carlo simulations with the Gupta potential *[23, 24]* was run using initial different structures at different temperatures in order to generate a small dataset for the fitting. After getting 2000 clusters, we did an initial training using ANN. As DFT based MD simulations are computationally expensive and time consuming, we further integrated MD simulations with ANN weights to generate more data.

Using Broyden-Fletcher-Goldfarb-Shanno (BFGS) algorithm *[25]*, quenching of the structures was done and included in the dataset. We processed our data through a superimposing algorithm to eradicate repeated geometries *[15]*. Overall, we generated 10,620 clusters containing all the nanoparticles in the range of Au_{13} to Au_{60}. The entire dataset of 10620 clusters is shuffled and separated into small set of files containing 295 data points each. 9145 data points are used for training and 1475 data points are utilized for testing purpose. RMS error of energy and forces shows a very smooth decay with the iterations when fitting of the functions is done with ANN. Also, fitting done with our ANN method is very fast because only after two iterations, the error got converged. The converged energy and force error was 6.8 meV/atom and 99.3 meV/Å/atom respectively for the testing dataset.

Vienna Ab initio Simulation package (VASP) *[26-29]* was used to perform all the DFT calculations. The Perdew-Burke-Ernzerhof (PBE) *[30, 31]* functional has been used for treating electron-correlation at generalized gradient approximation (GGA) with plane wave basis set.

For the sampling of Brillouin zone, a gamma k-point (1×1×1) mesh is used. The cell size for all clusters is taken as $22\times22\times22$ $Å^3$ with a constant vacuum dimension of 11 Å. The gradient convergence is set as 10^{-4} and threshold energy as 250 eV.

2.5. Validation of the ANN weights:

The validation of the obtained weights was done on a set of 400 clusters in the range of Au_{13}-Au_{60}. These clusters were not included in the training set. A plot of energy obtained using DFT and ANN for these clusters is shown in Fig.2. It can be seen that the DFT and ANN predicted energies are in agreement with each other and therefore the optimized weights can be applied to a wide range of clusters.

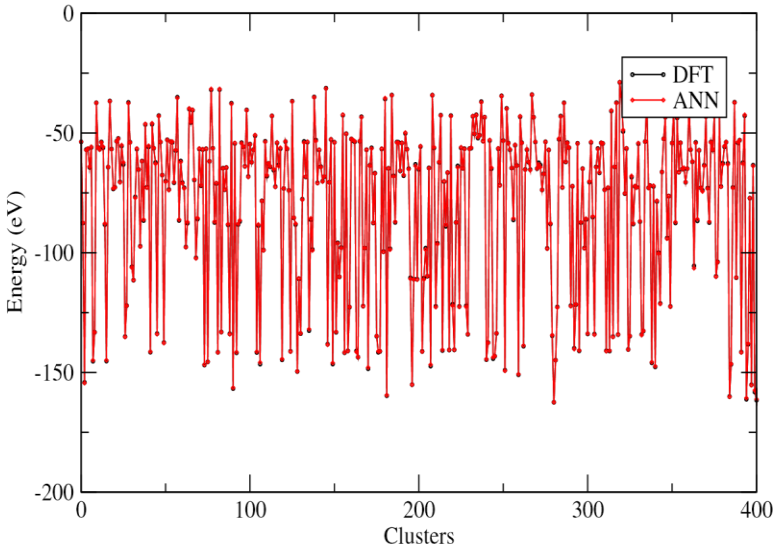

Figure 2: Comparison of energies obtained from DFT and ANN for a set of clusters in the range Au_{13}-Au_{60}.

In order to verify the capability of ANN in capturing the dependence of potential energy on bond length, we plotted a two dimensional PES for Au_{22} cluster as shown in Fig.3. In order to do this, we selected an optimized cluster of Au_{22}. One of the bond length between two selected atoms was varied from 1.9 Å to 10.0 Å. It is thus observed from Fig.3 that ANN is capable to differentiate between attractive, equilibrium and repulsive region of PES. This shows that ANN is a robust tool for fitting PES of gold

nanoclusters.

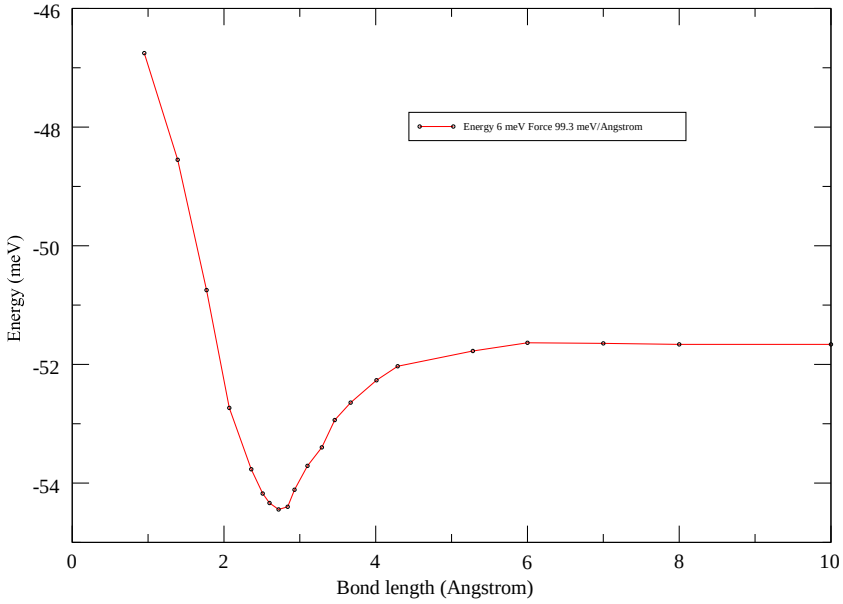

Figure 3: A two dimensional PES for Au_{22} obtained from optimized set of weights.

Chapter 3

Result and discussions

3.1. Search for the GM structure:

We have performed a GM search for Au_{55} using basin hopping (BH) method *[32]*.Initially, eight different structures was taken and their global optimization was done using BH method. After BH run, we got 400 structures which were refined and similar isomers were removed. We selected some clusters from the refined structures and ran MD simulations for them. We repeated the process until we got some good results. Overall, with BH method we have generated around 1000 geometries.

Apart from the BH calculations, we ran MD simulations at different temperatures 300 K, 400 K, 550 K and 700 K using ICO geometry of Au_{55} as the initial structure for approximately 1 million steps at a time step of 1 fs. From MD simulations, we quenched different structures and further used them as the initial structures for global optimizations. The obtained GM structure was disordered and less symmetrical. A reduction in the core size from 13 to 8 was observed. The surface atoms increased to 47. The structure of GM and core region is shown in Fig.5 and Fig.4 (a) respectively. In our study, we have found that the inner core structure of the predicted GM resembles with the innermost core structure of the GM of Au_{147} (Fig.4(c)) *[16]*; the only difference being that Au_{147} has 7 inner core atoms while Au_{55} has 8 atoms. Also, innermost core structure (Fig.4(c)) of the GM of Au_{147} is resembling exactly with the inner core structure of the reported GM (Fig.4 (b)) Au_{55}. The inner core of the predicted GM shows 8 atoms arranged in a capped square bi-pyramidal shape.

Table 3: MD simulations using different core atoms at time step of 1fs.

No. of core atoms	Temp. given (K)	MD steps run (in million)
4	300,450,600	0.2
6	300,450,600	0.2
7	300,400,500,600	0.8
8	300,400,550,700	1.0
9	300,400,550,700	0.2

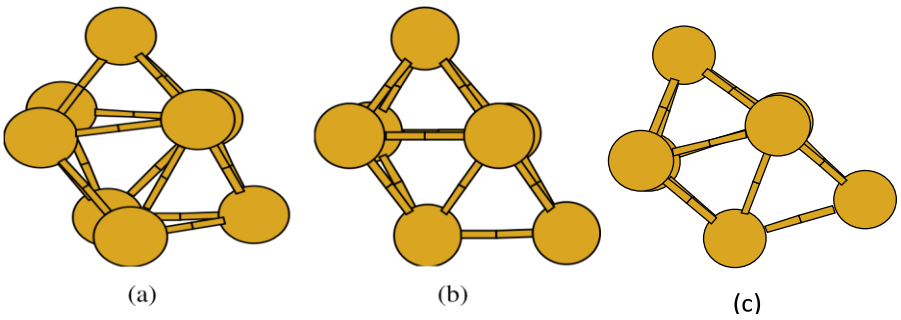

Figure 4: The inner core geometry for a) 8 atom inner core of predicted GM Au_{55} (side view), b) 7 atom inner core of reported GM Au_{55} (side view), c) 7 atom inner core of reported GM Au_{147} (top view).

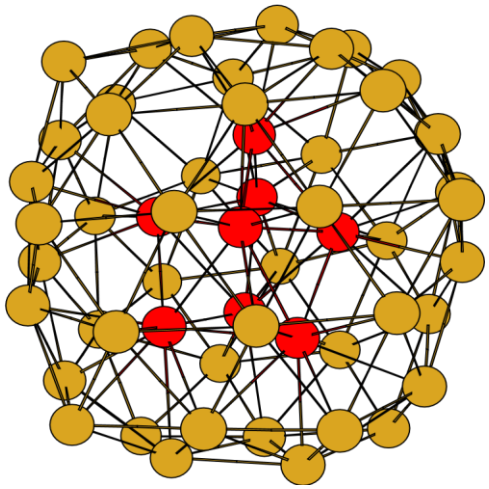

Figure 5: Predicted GM of Au_{55}.

3.2. Relative Total Energy:

We have calculated the relative total energy difference (ΔE_{dif}) for GM and low-lying structures (E_x) with respect to the ICO structure (E_{ICO}), that is, $\Delta E_{dif} = | E_x - E_{ICO} |$. Recently, a GM structure was reported by Piotrowski et al. *[18]* containing 7 atoms in the core region (Fig. 4(b)) and 48 atoms on the surface. We have performed VASP optimizations with the same parameters using DFT + PBE for our predicted GM structure (8 core atom) and the reported GM structure (7 core atom) *[18]*. It was found that 8 core atom structure is 0.14 eV lower in energy than the reported structure. With ANN, we found the energy difference of 0.13 eV between the predicted GM and the reported GM, so our ANN results are also consistent with the DFT results. In addition, using DFT, our predicted GM is 2.22 eV (Table 4) lower in energy than the icosahedral geometry of Au_{55}.

Table 4: The energy difference at DFT and ANN level is calculated w.r.t. the energy of ICO geometry.

Geometry	$\Delta E_{tot,DFT}$ (eV)	$\Delta E_{tot,ANN}$ (eV)
Predicted GM	2.22	2.11
Reported GM	2.08	1.98

3.3. Exclusion of Spin Orbit Coupling (SOC):

Piotrowski et al. *[18]* have studied the 7 core atom geometry with three different combinations of basis sets which are (i) DFT + PBE, (ii) DFT + PBE + vdW, (iii) DFT + PBE + SOC. The energy difference obtained from using basis set (i) and (ii) i.e. $|\Delta E_{i-ii}|$ was 4.7 meV and using basis set (i) and (iii) i.e. $|\Delta E_{i-iii}|$ was 0.6 meV. Such difference is negligible for consideration and also no change was observed in the geometry of the GM. Therefore, in the present work, SOC was not included due to its negligible contribution and high computational cost.

3.4. Fluxionality:

We have tried to explore the PES for Au_{55} by performing MD simulations using different core atoms as the initial structures. After quenching those structures, we got 80 low-lying structures in the range of 0.5 eV energy difference from the predicted GM structure. We observed that maximum core atom obtained was 9 and no 10 core atom structure was obtained in the low-lying isomers range. To confirm this, we took the structure of the GM of Au_{58} *[15]* which contains 10 core atoms, and removed three surface atom and used for initial structure to run MD simulations. After MD simulation and optimization, we got the structure with 9 core atoms (Fig.6). However, in the 80 low-lying structures, majority of them contains 8 core atoms structure, few with 7 core atoms and very few with 6 and 9 core atoms structures. Some of them are shown in Fig.11.

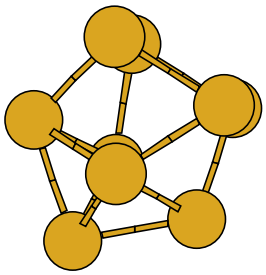

Figure 6: Core structure for Au_{55} after optimization from Au_{58}.

So, we can say that Au_{55} is highly fluxional in nature. Since, there is a considerable difference in the energy and the core structure arrangement of atoms, we can conclude that the structure of Au_{55} with 8 core atoms is the most stable geometry.

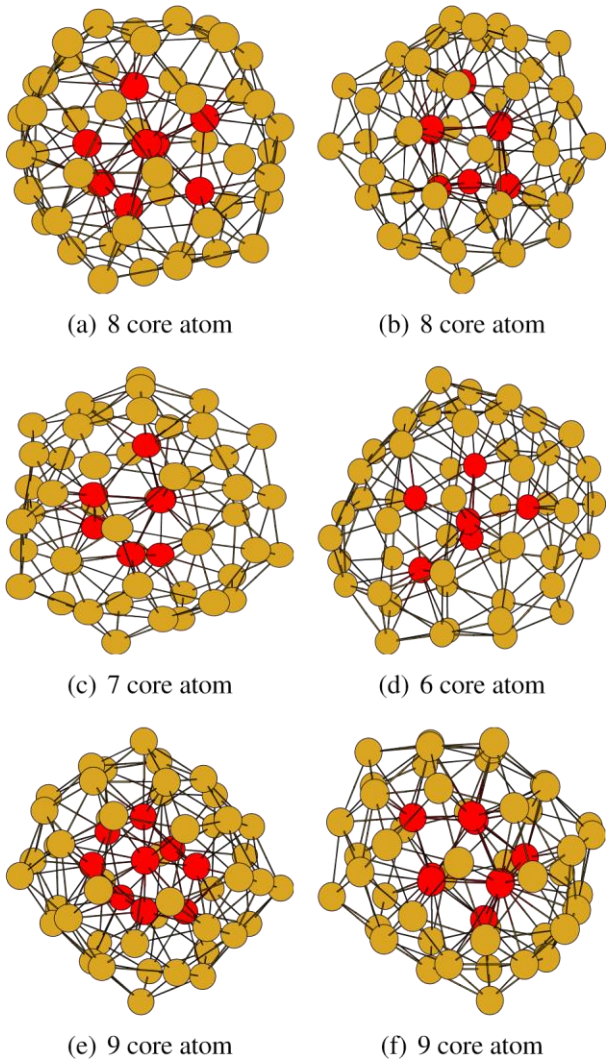

Figure 7: Some low-lying isomers of Au_{55} in the range of 0.5 eV energy difference from GM.

3.5. Probability distribution:

The physical and structural properties of nanoparticles are greatly affected by various parameters due to the changes which takes place at quantum level. Temperature is one of the key parameter which greatly effects the properties of nanoparticles. Probability distribution tells about the stability of the different isomers at a given temperature. The general equation of the probability is given by the Eq.8,

$$P = \frac{\exp\left(\frac{-\Delta E(N,V)}{k_b T}\right)}{Q(N,V,T)} \qquad \ldots\ldots\ldots (8)$$

Where, $Q(N,V,T)$ represents the partition function of the system. We have got the GM along with 80 low-lying isomers at an energy gap of 0.5 eV, so we have calculated the probability of each isomer at three temperatures - 300 K, 400 K and 700 K using the Li and Truhlar's method *[33]*. In this method, the probability of each isomer P_r is calculated by considering electronic, vibrational and rotational partition function and it can be summarized with the Eq.9,

$$\mathrm{P_r} = \frac{\exp\left(\frac{-\Delta \mathrm{E}}{\mathrm{k_b T}}\right) \mathrm{q^r_{rot} q^r_{vib} q^r_{ele}}}{\sum \exp\left(\frac{-\Delta \mathrm{E}}{\mathrm{k_b T}}\right) \mathrm{q^r_{rot} q^r_{vib} q^r_{ele}}} \qquad \ldots\ldots\ldots (9)$$

We have neglected the electronic transition term as these transitions are of very high energy and excited states have a negligible contribution to the partition function. Using the Rigid rotor approximations and harmonic approximations, P_r (Eq.9) can be modified as,

$$\mathrm{P_{m,r}} = \frac{\exp\left(\frac{-\Delta \mathrm{E}}{\mathrm{k_b T}}\right) \mathrm{q^r_{rot} q^r_{vib}}}{\sum \exp\left(\frac{-\Delta \mathrm{E}}{\mathrm{k_b T}}\right) \mathrm{q^r_{rot} q^r_{vib}}} \qquad \ldots\ldots\ldots (10)$$

Where, $P_{m,r}$ denotes the modified probability expression and q^r_{rot} and q^r_{vib} are given by Eq.11 and Eq.12,

$$q_{rot}^{r} = \left(\frac{8\pi^2}{\beta h^2}\right)\frac{\sqrt{\Pi\, I_a^r\, I_b^r\, I_c^r}}{\sigma^r} \qquad \ldots\ldots\ldots (11)$$

$$q_{vib}^{r} = \prod_{n}\frac{\exp\left(\frac{-hc\tilde{\nu}_j^i}{2k_bT}\right)}{1-\exp\left(\frac{-hc\tilde{\nu}_j^i}{K_bT}\right)} \qquad \ldots\ldots\ldots (12)$$

where $\tilde{\upsilon}$ is the wave number of the n^{th} normal mode of an isomer and I_a^r, I_b^r, I_c^r are the three principle moments of inertia of the isomer.

So, the probability of all low-lying isomers of Au_{55} is calculated and plotted (Fig.8). We got family of 8 core atoms isomer and 7 core atoms isomers in the low-lying isomers range. The family of 8 core atom isomers is most probable then the 7 core atom family. It can be observed from the graph that the predicted GM is the most stable structure below 700 K. After 700 K, isomer no.20 (Fig.10) starts gaining more probability as compared to other isomers and overcome the GM at 750 K which can be seen from Fig.9. All the isomers after energy difference of 0.39 eV from the predicted GM, are approximately equally probable at all three temperatures. The probability of 5 most probable low-lying isomers (isomer no. 9 as P_1, 15 as P_2, 18 as P_3, 20 as P_4, 52 as P_5) and the GM is summarized in the Table 8. As inner core of predicted GM is more symmetrical compared to reported GM, so we can interpret that the predicted GM has more probability than the reported GM at all temperatures.

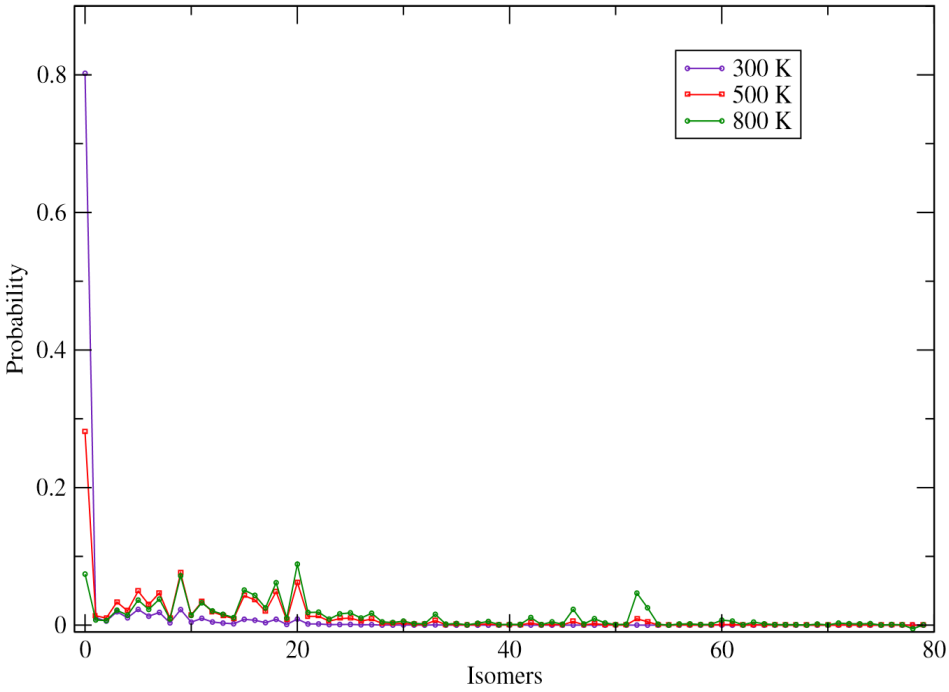

Figure 8: Probability plot of all low-lying isomers of Au_{55} at different temperatures.

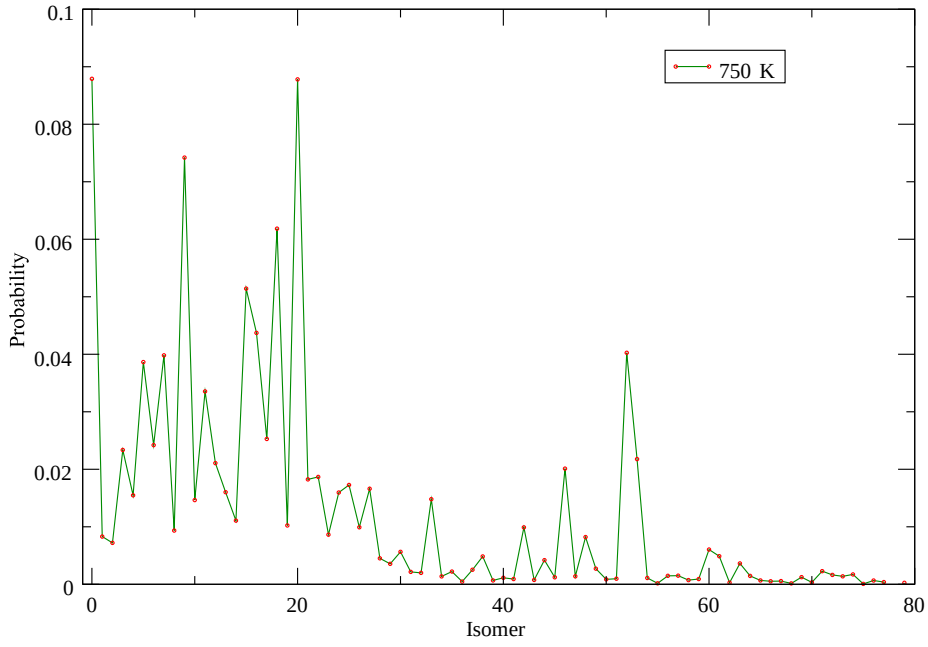

Figure 9: Probability of the predicted GM lowered down at higher temperature.

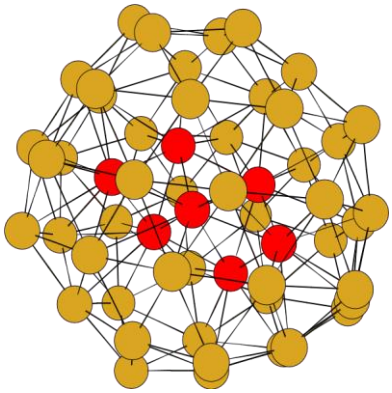

Figure 10: Geometry of low-lying isomer no. 20.

Table 5: Probability of predicted GM and 5 most probable low-lying isomers of Au_{55}.

Temperature (in K)	P_{GM} (%)	P_1 (%)	P_2 (%)	P_3 (%)	P_4 (%)	P_5 (%)
300	80.24	2.26	0.85	0.85	0.88	0.01
500	28.09	7.60	4.29	4.85	6.21	0.92
800	7.42	7.17	5.09	6.17	8.87	4.65

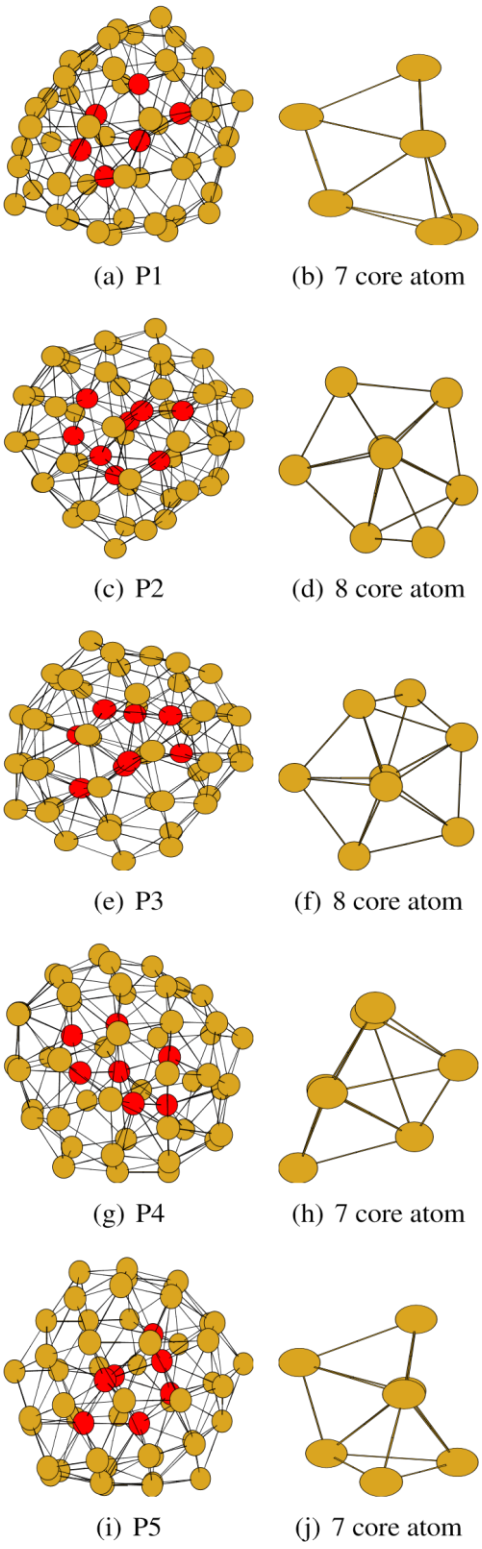

Figure 11: Geometry of 5 most probable isomers (left side) and their respective core geometry (right side).

Chapter 4

Conclusions

In this work, the dynamics of Au_{55} NC is studied theoretically using ANN potential and the fitting of PES is done with this potential for the cluster ranging from Au_{13} to Au_{60} with an accuracy of 6.8 meV/atom for energy and 99.3 (meV/Å)/atom for the force calculations. For the GM search of Au_{55}, BH method is used along with MD simulations at different temperatures. In the energy calculation of GM, SOC is not included. The predicted GM consists of symmetric core of 8 atoms and surface is disordered as compared to the ICO which is highly symmetric configuration. Fluxional behavior of Au_{55} is confirmed by 80 low-lying isomers. The unsymmetrical surface of GM attracts various catalytic applications [34-38]. The predicted GM is found to be 2.22 eV stable in energy than ICO. On going from Au_{55} to Au_{147}, core atoms reduced from 8 to 7, may be due to the repulsion of core atoms in Au_{147}.

REFERENCES

[1] P. Pyykko, (1988), Relativistic effects in structural chemistry, Chem. Rev., 88, 563–594, (DOI: 10.1021/cr00085a006).

[2] M. Jansen, (2005), Effects of relativistic motion of electrons on the chemistry of gold and platinum, Sol. St. Sci., 7, 1464–1474, (DOI: 10.1016/j.solidstatesciences.2005.06.015).

[3] P. Schwerdtfeger, M. Dolg, G. A. Bowmaker, W. E. Schwarz, P. D. Boyd, (1989), Relativistic effects in gold chemistry. I. Diatomic gold compounds, J. Chem. Phys., 91, 1762–1774, (DOI: 10.1063/1.457082).

[4] X. Huang, Y. Luo, Z. Li, B. Li, H. Zhang, L. Li, I. Majeed, P. Zuo, B. Tan, (2011), Biolabeling hematopoietic system cells using near-infrared fluorescent gold nanoclusters, Jour. of Phy. Chem., 115, 16753–16763, (DOI: 10.1021/jp202612p).

[5] G. Li, R. Jin, (2013), Atomically precise gold nanoclusters as new model catalysts, Acc. Chem. Res., 46, 1749–1758, (DOI: 10.1021/ar300213z).

[6] R. Sardar, A. M. Funston, P. Mulvaney, R. W. Murray, (2009), Gold Nanoparticles: Past, Present, and Future, Langmuir, 25, 13840– 13851, (DOI: 10.1021/la9019475).

[7] X. Wu, X. He, K. Wang, C. Xie, B. Zhou, Z. Quing, (2010), Ultrasmall near-infrared gold nanoclusters for tumor fluorescence imaging in vivo, Nanoscale, 2, 2244–2249, (DOI: 10.1039/C0NR00359J).

[8] J. Stehr, C. Hrelescu, R. A. S. G. Raschke, M. Wunderlich, A. Nichtl, D. Heindl, K. Kürzinger, W. J. Parak, T. A. Klar, J. Feldmann, (2008), Gold Nano Stoves for Microsecond DNA Melting Analysis, Nano Lett., 8, 619–623, (DOI: 10.1021/nl073028i).

[9] S. Goedecker, (2004), Minima hopping: An efficient search method for the global minimum of the potential energy surface of complex molecular systems, J. Chem. Phys., 120, 9911, (DOI: 10.1063/1.1724816).

[10] G. H. Johannesson, T. Bligaard, A. V. Ruban, H. L. Skriver, K. W. Jacobsen, J. K. Nörskov, (2002), Combined Electronic Structure and Evolutionary Search Approach to Materials Design, Phys. Rev. Lett., 88, 255506, (DOI: 10.1103/PhysRevLett.88.255506).

[11] S. Chiriki, S. Jindal, S. S. Bulusu, (2017), c-T phase diagram and Landau free energies of $(AgAu)_{55}$ nanoalloy via neural-network molecular dynamic simulations, J. Chem. Phys., 147, 154303, (DOI: 10.1063/1.4998319).

[12] P. Salomon, P. Sibani, R. Frost, (2002), Facts, Conjectures and Improvements for Simulated Annealing, SIAM, Philaelphia, (ISBN: 0-89871-508-3).
[13] B. A. Berg, T. Neuhaus, (1991), Multicanonical algorithms for first order phase transitions, Phys. Lett. B, 267, 249–253, (DOI: 10.1016/0370-2693(91)91256-U).
[14] D. J. Wales, J. P. Doye, (1997), Global Optimization by Basin-Hopping and the Lowest Energy Structures of Lennard-Jones Clusters Containing up to 110 Atoms, J. Phys. Chem. A, 101, 5111–5116, (DOI: 10.1021/jp970984n).
[15] S. Chiriki, S. Jindal, S. S. Bulusu, (2017), Neural network potentials for dynamics and thermodynamics of gold nanoparticles, J. Chem. Phys., 146, 084314, (DOI: 10.1063/1.4977050).
[16] S. Jindal, S. Chiriki, S. S. Bulusu, (2017), Spherical harmonics based descriptor for neural network potentials: Structure and dynamics of Au_{147} nanocluster, J. Chem. Phys., 146, 204301, (DOI: 10.1063/1.4983392).
[17] A. L. Mackay, (1962), A dense non-crystallographic packing of equal spheres, Acta Crystallogra., 15, 916–918.
[18] M. J. Piotrowski, C. G. Ungureanu, P. Tereshchuk, K. E. Batista, A. S. Chaves, D. Guedes-Sobrinho, J. L. D. Silva, (2016), Theoretical Study of the Structural, Energetic, and Electronic Properties of 55-Atom Metal Nanoclusters: A DFT Investigation within van der Waals Corrections, Spin–Orbit Coupling, and PBE+U of 42 Metal Systems, J. Phys. Chem. C, 120, 28844–28856, (DOI: 10.1021/acs.jpcc.6b10404).
[19] I. L. Garzón, M. Beltrán, G. González, J. A. Reyes-Nava, I. Gutíerrez-González, K. Michaelian, J. I. Rodríguez-Hernández, (2003), Chirality, defects, and disorder in gold clusters, Eur. Phys. Jour. D, 24, 105–109, (DOI: 10.1140/epjd/e2003-00187-4).
[20] Z. W. Wang, R. E. Palmer, (2012), Experimental Evidence for Fluctuating, Chiral-Type Au_{55} Clusters by Direct Atomic Imaging, Nano Lett., 12, 5510–5514, (DOI: 10.1021/nl303429z).
[21] A. P. Bartók, R. Kondor, G. Csányi, (2013), On representing chemical environments, Phys. Rev. B, 87, 184115, (DOI: 10.1103/PhysRevB.87.184115).
[22] J. Behler, (2015), Constructing high-dimensional neural network potentials: A tutorial review, Int. J. Quant. Chem., 115, 1032, (DOI: 10.1002/qua.24890).
[23] R. P. Gupta, (1981), Lattice relaxation at a metal surface, Phys. Rev. B, 23, 6265, (DOI: 10.1103/PhysRevB.23.6265).

[24] A. Bruma, R. Ismail, L. O. Paz-Borbon, H. Arslan, G. Barcaro, A. Fortunelli, Z. Y. Li, R. L. Johnston, (2013), DFT study of the structures and energetics of 98-atom AuPd clusters, Nanoscale, 5, 646, (DOI: 10.1039/C2NR32517A).
[25] Y. X. Yuan, (1991), A Modified BFGS Algorithm for Unconstrained Optimization, IMA Jour. of Num. Ana., 11, 325–332, (DOI: 10.1093/imanum/11.3.325).
[26] G. Kresse, J. Hafner, (1993), Ab initio molecular dynamics for liquid metals, Phys. Rev. B, 47, 558, (DOI: 10.1103/PhysRevB.47.558).
[27] G. Kresse, J. Hafner, (1994), Ab initio molecular-dynamics simulation of the liquid-metal–amorphous-semiconductor transition in germanium, Phys. Rev. B, 49, 14251, (DOI: 10.1103/PhysRevB.49.14251).
[28] G. Kresse, J. Furthmüller, (1996), Efficiency of ab-initio total energy calculations for metals and semiconductors using a plane-wave basis set, Comp. Mat. Sci., 6, 15-50, (DOI: 10.1016/0927-0256(96)00008-0).
[29] G. Kresse, J. Furthmüller, (1996), Phys. Rev. B, 54, 11169.
[30] J. P. Perdew, K. Burke, M. Ernzerhof, (1996), Generalized Gradient Approximation Made Simple, Phys. Rev. Lett., 77, 3865, (DOI: 10.1103/PhysRevLett.77.3865).
[31] J. P. Perdew, K. Burke, M. Ernzerhof, (1997), The adiabatic connection method: a non-empirical hybrid, Chem. Phys. Lett., 265, 115-120, (DOI: 10.1016/S0009-2614(96)01373-5).
[32] D. J. Wales, H. A. Scheraga, (1999), Global Optimization of Clusters, Crystals, and Biomolecules, Science, 285, 1368, (DOI: 10.1126/science.285.5432.1368).
[33] Z. H. Li, D. G. Truhlar, (2014), Nanothermodynamics of metal nanoparticles, Chem. Sci., 5, 2605, (DOI: DOI: 10.1039/C4SC00052H).
[34] M. Haruta, (1997), Size- and support-dependency in the catalysis of gold, Catal. Today, 36, 153–166, (DOI: 10.1016/S0920-5861(96)00208-8).
[35] B. Hvolbæk, T. V. Janssens, B. S. Clausen, H. Falsig, C. H. Christensen, J. K. Nørskov, (2007), Catalytic activity of Au nanoparticles, Nano Today, 2, 14, (DOI: 10.1016/S1748-0132(07)70113-5).
[36] M. S. Chen, D. W. Goodman, (2004), The Structure of Catalytically Active Gold on Titania Science, 306, 252, (DOI: 10.1126/science.1102420).
[37] M. Haruta, M. Daté, (2001), Advances in the catalysis of Au nanoparticles, Appl. Catal. A, 222, 427–437, (DOI: 10.1016/S0926-860X(01)00847-X).

[38] H. Häkkinen, (2008), Atomic and electronic structure of gold clusters: understanding flakes, cages and superatoms from simple concepts, Chem. Soc. Rev., 37, 1847, (DOI: 10.1039/B717686B).